

4-1-2019

STING-mediated disruption of calcium homeostasis chronically activates ER stress and primes T cell death

Jianjun Wu
University of Texas Southwestern Medical Center

Yu-Ju Chen
University of Texas Southwestern Medical Center

Nicole Dobbs
University of Texas Southwestern Medical Center

Tomomi Sakai
University of Texas Southwestern Medical Center

Jen Liou
University of Texas Southwestern Medical Center

See next page for additional authors

Follow this and additional works at: https://digitalcommons.wustl.edu/open_access_pubs

Recommended Citation

Wu, Jianjun; Chen, Yu-Ju; Dobbs, Nicole; Sakai, Tomomi; Liou, Jen; Miner, Jonathan J.; and Yan, Nan, "STING-mediated disruption of calcium homeostasis chronically activates ER stress and primes T cell death." *Journal of Experimental Medicine*. 216,4. . (2019).
https://digitalcommons.wustl.edu/open_access_pubs/8566




This Open Access Publication is brought to you for free and open access by Digital Commons@Becker. It has been accepted for inclusion in Open Access Publications by an authorized administrator of Digital Commons@Becker. For more information, please contact vanam@wustl.edu.

Authors

Jianjun Wu, Yu-Ju Chen, Nicole Dobbs, Tomomi Sakai, Jen Liou, Jonathan J. Miner, and Nan Yan

ARTICLE

STING-mediated disruption of calcium homeostasis chronically activates ER stress and primes T cell death

Jianjun Wu^{1,2}, Yu-Ju Chen³, Nicole Dobbs^{1,2}, Tomomi Sakai^{1,2}, Jen Liou³ , Jonathan J. Miner^{4,5,6} , and Nan Yan^{1,2} 

STING gain-of-function mutations cause lung disease and T cell cytopenia through unknown mechanisms. Here, we found that these mutants induce chronic activation of ER stress and unfolded protein response (UPR), leading to T cell death by apoptosis in the *Sting*^{N153S/+} mouse and in human T cells. Mechanistically, STING-N154S disrupts calcium homeostasis in T cells, thus intrinsically primes T cells to become hyperresponsive to T cell receptor signaling-induced ER stress and the UPR, leading to cell death. This intrinsic priming effect is mediated through a novel region of STING that we name “the UPR motif,” which is distinct from known domains required for type I IFN signaling. Pharmacological inhibition of ER stress prevented *Sting*^{N153S/+} T cell death in vivo. By crossing *Sting*^{N153S/+} to the *OT-1* mouse, we fully restored CD8⁺ T cells and drastically ameliorated STING-associated lung disease. Together, our data uncover a critical IFN-independent function of STING that regulates calcium homeostasis, ER stress, and T cell survival.

Introduction

Innate immune recognition of invading pathogens is the first line of defense in mammalian cells that activates type I IFN and inflammatory responses. One important protein that plays a central role in sensing a wide range of microbial pathogens is stimulator of IFN genes (STING). STING is a transmembrane protein localized on the ER. STING is best known as the non-redundant adaptor protein downstream of cytosolic DNA sensing (of DNA viruses and retroviruses; Yan et al., 2010; Gao et al., 2013; Sun et al., 2013). The DNA sensor cyclic GMP-AMP synthase (cGAS) binds double-stranded DNA and converts ATP and GTP into 2'3' cyclic GMP-AMP (cGAMP). cGAMP acts as a second messenger that binds STING on the ER and triggers IFN signaling (Sun et al., 2013; Wu et al., 2013). STING is also critical for direct sensing of bacterial cyclic dinucleotide (CDN; Burdette et al., 2011). The cGAS–STING pathway has also been implicated in several monogenic autoimmune diseases, such as Aicardi-Goutières syndrome, caused by defective nucleases such as TREX1/DNase III and RNaseH2 (Pokatayev et al., 2016; Yan, 2017).

Besides its role in antimicrobial defense, several gain-of-function mutations in *TMEM173* encoding STING have been

reported in STING-associated vasculopathy with onset in infancy (SAVI) as well as in patients with systemic lupus erythematosus-like syndromes or familial chilblain lupus (Jeremiah et al., 2014; Liu et al., 2014; König et al., 2017; Melki et al., 2017). We and others showed that these mutations constitutively activate STING trafficking and signaling independent of ligand binding (Dobbs et al., 2015; Melki et al., 2017). We also generated a heterozygous *Sting*-N153S (N154S in human STING) knock-in mouse as a model for SAVI (Warner et al., 2017). These mice spontaneously develop inflammation in the lung, T cell cytopenia, and premature death, closely mimicking pathological findings in human SAVI patients. Another gain-of-function mutant mouse, *Sting*-V154M (V155M in human STING), also develops severe immunodeficiency (Bouis et al., 2018). We showed that, surprisingly, *Sting*-N153S mice lacking IRF3 also develop lung disease and T cell cytopenia, which suggested an unknown IRF3/IFN-independent function of STING in SAVI disease pathogenesis, at least in the mouse. Interestingly, a large portion of the STING protein is evolutionarily conserved in most animal phyla, including unicellular organisms, although the C-terminal tail required for tank-binding kinase 1 (TBK1) and IRF3 binding

¹Department of Immunology, University of Texas Southwestern Medical Center, Dallas, TX; ²Department of Microbiology, University of Texas Southwestern Medical Center, Dallas, TX; ³Department of Physiology, University of Texas Southwestern Medical Center, Dallas, TX; ⁴Department of Medicine, Washington University School of Medicine, St. Louis, MO; ⁵Department of Molecular Microbiology, Washington University School of Medicine, St. Louis, MO; ⁶Department of Pathology and Immunology, Washington University School of Medicine, St. Louis, MO.

Correspondence to Nan Yan: nan.yan@utsouthwestern.edu.

© 2019 Wu et al. This article is distributed under the terms of an Attribution–Noncommercial–Share Alike–No Mirror Sites license for the first six months after the publication date (see <http://www.rupress.org/terms/>). After six months it is available under a Creative Commons License (Attribution–Noncommercial–Share Alike 4.0 International license, as described at <https://creativecommons.org/licenses/by-nc-sa/4.0/>).

and IFN signaling is only present in vertebrate and mammals (Margolis et al., 2017). An IFN-independent function of STING has not been well defined.

Here, we investigated the mechanism by which STING gain-of-function mutant causes T cell death and lung disease. We uncovered a critical IFN-independent function of STING, mediated through a previously uncharacterized motif, which regulates calcium homeostasis, ER stress, and T cell survival. We also found that TCR signaling synergizes with ER stress in the *Sting*^{N153S/+} mouse, leading to T cell death, inflammation, and lung disease. Thus, our study reveals an important new function of STING signaling in balancing life and death decisions of a T cell during development, with broad implications on immune and tissue homeostasis.

Results

Gain-of-function STING mutation causes T cell activation and cell death in the *Sting*^{N153S/+} mouse

To understand how *Sting*-N153S knock-in mutation in mice causes T cell cytopenia, we first assessed whether T cells in the *Sting*^{N153S/+} mouse undergo spontaneous cell death. We previously showed that *Sting*^{N153S/+} mice contain significantly fewer T cells in the spleen as well as substantially reduced thymus size compared with littermate WT mice (Warner et al., 2017). To analyze the remaining T cells in *Sting*^{N153S/+} mice, we stained CD3⁺ T cells from the spleen for annexin V or activated caspases (using the CaspACE FITC-VAD-FMK dye) to measure cell death by FACS. *Sting*^{N153S/+} CD3⁺ T cells showed substantially increased staining for both cell death markers compared with littermate WT T cells (Fig. 1 A). Both cell death markers were also significantly increased in CD4⁺ and CD8⁺ *Sting*^{N153S/+} compared with littermate WT T cells (Fig. 1 A). We next analyzed biochemical markers of apoptosis in WT and *Sting*^{N153S/+} T cells, which showed a strong presence of cleaved caspase 3 in *Sting*^{N153S/+} but not WT T cells (Fig. 1 B). Caspase activation is associated with BH3-only protein expression, among which BCL2 is an anti-apoptotic member, whereas Noxa and Bik play pro-apoptotic roles. We found that *Bcl2* mRNA expression was significantly decreased while *Noxa* and *Bik* mRNA expressions were significantly increased in *Sting*^{N153S/+} compared with WT T cells (Fig. 1 B). These data suggest that T cells in *Sting*^{N153S/+} mice are undergoing spontaneous cell death.

To investigate *Sting*^{N153S/+} T cell death phenotype further, we assessed T cell activation markers in littermate WT and *Sting*^{N153S/+} splenic T cells by FACS. CD69 is elevated in both CD4⁺ and CD8⁺ T cells of *Sting*^{N153S/+} compared with littermate WT mice (Fig. 1 C). Naive T cells (CD44^{lo}CD62^{hi}) are reduced and antigen-experienced T cells (CD44^{hi}) are increased in *Sting*^{N153S/+} mice compared with WT (Fig. 1 D). CD44^{hi} T cells from *Sting*^{N153S/+} mice also were positive for activated caspases (Fig. 1 E), suggesting that these activated T cells are undergoing cell death. We next evaluated how WT and *Sting*^{N153S/+} T cells respond to TCR signaling ex vivo. WT T cells underwent rapid proliferation after CD3/CD28 antibody stimulation, whereas *Sting*^{N153S/+} T cells did not proliferate and instead engaged in cell death (Fig. 1 F and G). Moreover, WT T cells treated with STING

agonist 5,6-dimethylxanthenone-4-acetic acid (DMXAA; a cell-permeable small molecule) also failed to proliferate and engaged in cell death after CD3/CD28 antibody stimulation (Fig. 1 H and I). Taken together, these observations suggest that *Sting*^{N153S/+} T cell death is associated with T cell activation and proliferation, and additional TCR stimulation further enhances N153S T cell death. Activated caspases were selectively detected in activated but not naive *Sting*^{N153S/+} T cells within the same population, suggesting a cell-intrinsic mechanism for *Sting*^{N153S/+} T cell activation and cell death.

Chronic activation of ER stress in *Sting*^{N153S/+} T cells

The above observations prompted us to hypothesize that T cell activation by TCR signaling promotes T cell death in *Sting*^{N153S/+} mice. TCR signaling not only activates T cell but it also induces ER stress and the unfolded protein response (UPR; Pino et al., 2008), and prolonged ER stress can prime cells to commit cell death. We therefore performed Western blot to detect UPR proteins in total splenic T cells from WT and *Sting*^{N153S/+} mice. Remarkably, we found that multiple UPR proteins such as Bip and Chop were strongly elevated in *Sting*^{N153S/+} compared with WT T cells (Fig. 2 A), suggesting chronic activation of ER stress and the UPR in *Sting*^{N153S/+} T cells in vivo. In comparison, Bip and Chop protein levels were only slightly increased in *Sting*^{N153S/+} B cells compared with WT B cells and did not change in *Sting*^{N153S/+} macrophages compared with WT macrophages (Fig. 2 A). Of note, WT B cells expressed surprisingly high basal levels of UPR proteins for unknown reasons. In accordance with the ER stress phenotype, we detected a strong signal of cleaved caspase 3 only in T cells as well as a detectable but much less robust signal in B cells and no caspase 3 cleavage in macrophages (Fig. 2 A). We also did not observe increased UPR proteins in *Sting*^{N153S/+} monocytes (Fig. S1 A), *Sting*^{N153S/+} MEFs, or *STING*^{N154S} skin fibroblasts isolated from two independent SAVI patients (Fig. 2 B). We next analyzed various mouse tissues, and only spleen showed elevated UPR and caspase 3 cleavage in *Sting*^{N153S/+} compared with WT mice (Fig. S1 B). These results demonstrate that T cells are selectively affected by *Sting*-N153S-mediated UPR activation and cell death.

We next stimulated WT and *Sting*^{N153S/+} T cells with CD3/CD28 antibodies and evaluated UPR and caspase activation by Western blot. CD3/CD28 antibody stimulation of WT T cells activated the UPR (as measured by increased expression of Bip, Chop, and p-IRE1) but not caspase 3 cleavage (compare lane 1 and 3; Fig. 2 C), suggesting that WT T cells can tolerate TCR signaling-mediated ER stress and avoid cell death. Of note, the extents of UPR protein expression in WT T cell stimulated with CD3/CD28 antibodies were still lower than those in untreated *Sting*^{N153S/+} T cells (compare lane 2 and 3; Fig. 2 C). When *Sting*^{N153S/+} T cells were stimulated with CD3/CD28 antibodies, UPR proteins did not further increase, which likely had reached maximal levels, and we detected increased caspase 3 cleavage. These data indicate a synergistic effect of TCR signaling and ER stress associated with *Sting*^{N153S/+} in balancing proliferation and cell death decisions in T cells.

To examine whether reducing ER stress pharmacologically in *Sting*^{N153S/+} T cells can prevent cell death, we first treated WT and

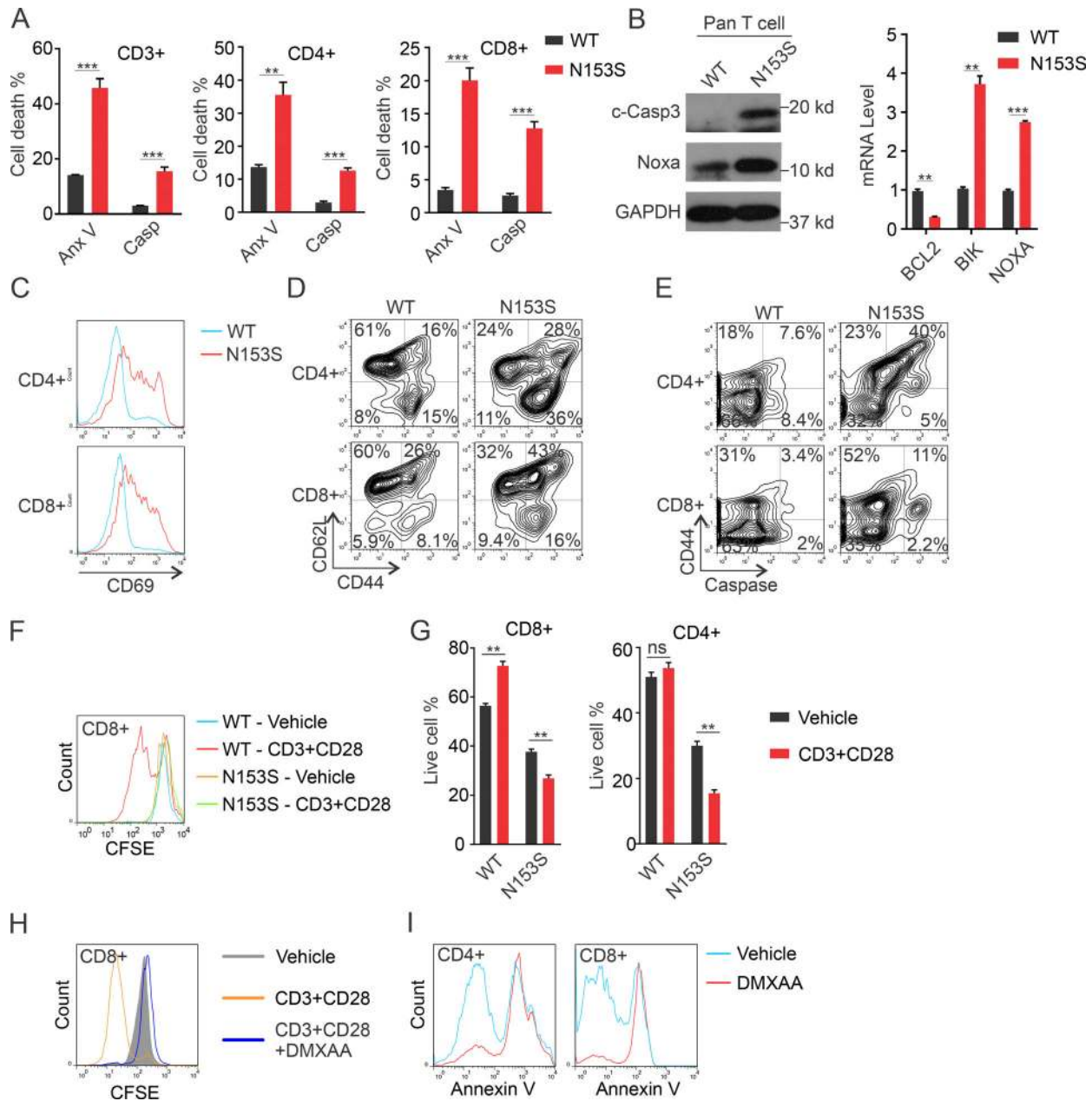


Figure 1. *Sting*^{N153S/+} mouse T cells undergo spontaneous activation and apoptotic cell death. (A) FACS analysis of T cell death. *Sting*^{N153S/+} or WT littermate mouse splenocytes were stained with T cell markers (α -CD3, CD4, or CD8 antibodies) and cell death markers (annexin V or CaspACE FITC-VAD-FMK). Frequencies of cell death of CD3⁺, CD4⁺, or CD8⁺ T cells were analyzed by FACS, and accumulated results from triplicate experiments are shown as bar graphs. Anx V, annexin V; Casp, caspase. (B) Immunoblots and qRT-PCR analysis of apoptosis markers in WT and *Sting*^{N153S/+} mouse T cells. Pan T cells were isolated from spleens of *Sting*^{N153S/+} or WT littermate mice. Indicated apoptotic protein and mRNA expression was analyzed by immunoblots (left) or qRT-PCR (right). Data are representative of at least three independent experiments. (C-E) FACS analysis of WT and *Sting*^{N153S/+} mouse T cell activation and cell death. Fresh isolated splenocytes from *Sting*^{N153S/+} or WT littermate mice were stained with CD4 and CD8 antibodies and T cell activation markers CD69 (C), activation marker CD44 and CD62L (D), or activation marker CD44 and cell death marker caspase (CaspACE FITC-VAD-FMK; E), then analyzed by FACS. (F and G) FACS analysis of mouse T cell proliferation and cell death. *Sting*^{N153S/+} or WT littermate mouse splenocytes were stained with CFSE first, then either mock treated or stimulated with CD3/CD28 antibodies for 3 d. The cell proliferation of CD8⁺ T cells was analyzed by CFSE dilution (F). In separate experiments, splenocytes were stimulated with or without CD3/CD28 antibodies for 1 d, then CD4⁺ or CD8⁺ T cells were analyzed by annexin V staining (G). (H and I) FACS analysis of T cell proliferation and cell death after STING agonist DMXAA treatment. WT splenocytes were stained with CFSE first, then either mock treated or stimulated with DMXAA in the presence or absence of CD3/CD28 antibodies for 3 d. CD8⁺ T cell proliferation was analyzed by CFSE dilution as in F. Annexin V staining of CD4⁺ or CD8⁺ T cells was also done similar to G. Error bars, SEM. **, P < 0.01; ***, P < 0.001; ns, not significant. Student's *t* test. Data in all panels are representative of at least three independent experiments.

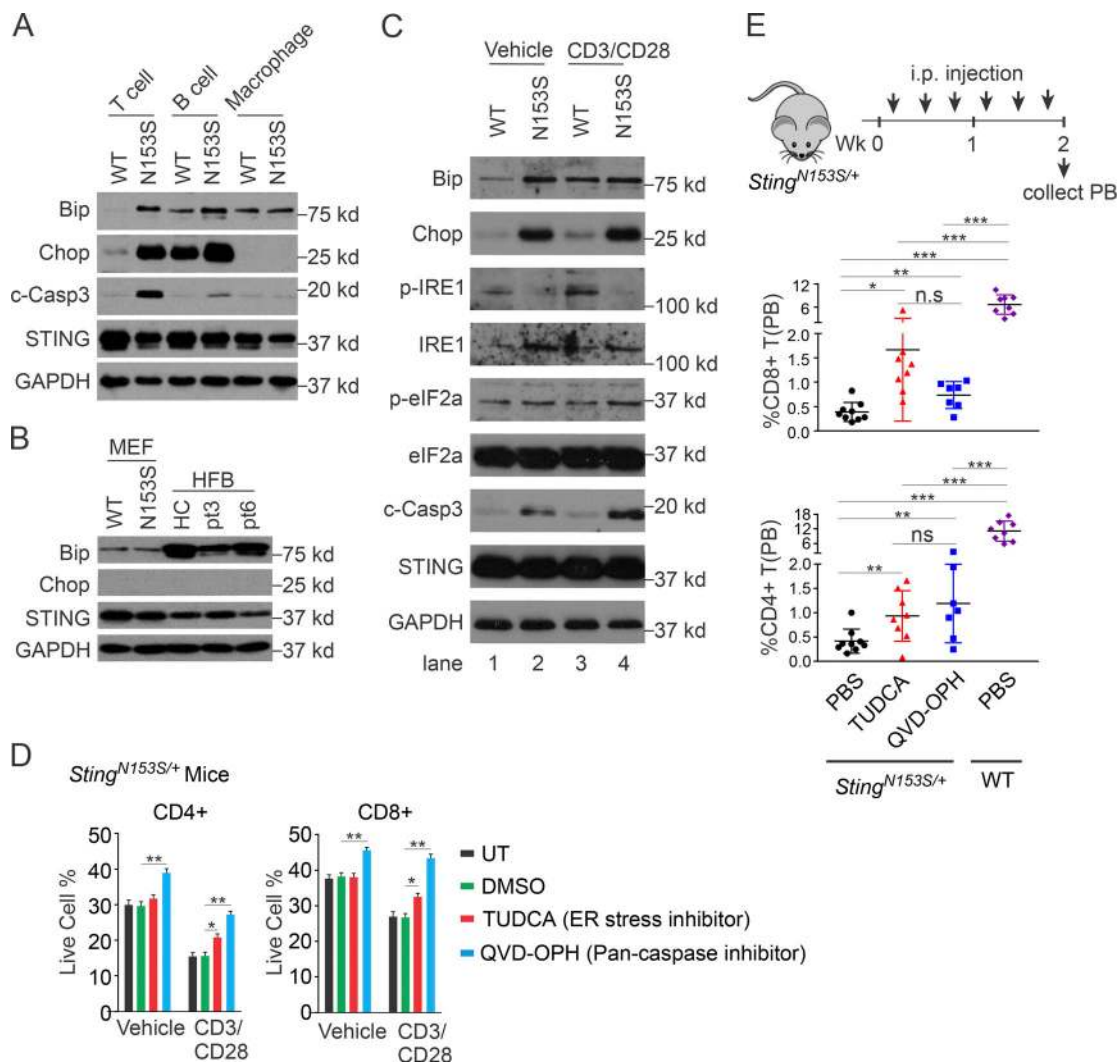


Figure 2. Chronic activation of ER stress and the UPR induces T cell death in the *Sting*^{N153S/+} mouse. (A) Immunoblot analysis of the UPR and apoptosis in WT and *Sting*^{N153S/+} immune cells. T cells, B cells, and macrophages were isolated from littermate WT and *Sting*^{N153S/+} mice; and lysates from fresh isolated cells were used for immunoblot analysis of indicated proteins. (B) Immunoblot analysis of the UPR in primary MEFs or human fibroblasts (HFB). The primary MEF cells were isolated from WT and *Sting*^{N153S/+} E13.5 embryos. Human skin fibroblasts were isolated from a healthy donor control (HC) or two independent SAVI patients (pt3 and pt6; Liu et al., 2014). (C) Immunoblot analysis of the UPR and apoptosis in WT and *Sting*^{N153S/+} T cells. Pan T cells from littermate WT and *Sting*^{N153S/+} mice were either mock treated (Vehicle) or stimulated with CD3/CD28 antibodies for 3 h. Lysates from treated cells were used for immunoblot analysis of indicated proteins. (D) FACS analysis of cell proliferation and cell death. Pan T cells were isolated from WT and *Sting*^{N153S/+} mice, then either untreated (UT) or mock treated (DMSO) or treated with TUDCA or QVD-OPH in the presence or absence of CD3/CD28 antibodies. The cells were then stained with CaspACE FITC-VAD-FMK In Situ Marker and analyzed by FACS. (E) In vivo treatment of *Sting*^{N153S/+} mice. Top: schematic diagram of the experimental design. Bottom: FACS analysis of CD4⁺ and CD8⁺ T cells in mouse peripheral blood (PB). *Sting*^{N153S/+} mice were i.p. injected with PBS, TUDCA (250 mg/kg, three injections per wk), or QVD-OPH (10 mg/kg, three injections per wk). T cells from the peripheral blood were analyzed after 14 d. n = 8–10. Error bars: SEM; *, P < 0.05; **, P < 0.01; ***, P < 0.001; ns, not significant. Student's t test. Data shown are from a representative dataset from two repeat treatment experiments.

Sting^{N153S/+} T cells with tauroursodeoxycholic acid (TUDCA), a chemical chaperon that relieves ER stress, or a pan-caspase inhibitor QVD-OPH in the presence or absence of CD3/CD28 antibodies. Both TUDCA and QVD-OPH treatments protected *Sting*^{N153S/+} T cells from cell death by CD3/CD28 antibody stimulation, and QVD-OPH also increased survival of resting *Sting*^{N153S/+} T cells (Fig. 2 D). We next treated 6–8-wk-old *Sting*^{N153S/+} mice with TUDCA or QVD-OPH by i.p. injection (three times per wk for 2 wk) and analyzed T cells in the peripheral blood (Fig. 2 E). *Sting*^{N153S/+} peripheral blood contains very low levels of CD4⁺ and CD8⁺ T cells. Both TUDCA and

QVD-OPH significantly increased T cells in *Sting*^{N153S/+} peripheral blood after 2 wk of treatment; in some cases, CD8⁺ T cells rebounded to the WT level (Fig. 2 E). These data suggest that gain-of-function STING mutation-associated T cell death is mediated through chronically activated ER stress and the UPR and that pharmacological inhibition of ER stress could be an exciting avenue of therapy for SAVI.

Human STING-N154S primes T cell death through ER stress

To further dissect the cell-intrinsic molecular mechanism in human cells, we reconstituted the STING-N154S-induced T cell

death phenotype in human Jurkat T cells (hSTING N154 is the corresponding residue for mSting N153). We transduced WT Jurkat T cells with a lentivirus vector that allows doxycycline (Dox)-inducible expression of either Flag-tagged STING-WT or STING-N154S mutant at physiological levels comparable to the endogenous WT STING (N154S-low; Fig. S2 A, “N154S cells” below). Inducible expression of N154S at the physiological level did not activate detectable IFN or apoptotic signaling pathways in Jurkat T cells, whereas conventional overexpression activated both (Fig. S2, A and B). The lack of IFN signaling activation in Jurkat N154S cells mimics that of the *Sting*^{N153S/+} mice (Warner et al., 2017).

We hypothesized that N154S expression may intrinsically prime Jurkat T cells for cell death after TCR activation. Thus, we treated STING-WT and N154S cells (induced by Dox) with PMA +ionomycin (mimics TCR activation), and we used IncuCyte and a live-cell imaging-compatible caspase 3/7 dye to monitor cell death kinetics over time (see Materials and methods). PMA +ionomycin induced robust cell death only in N154S-expressing cells but not in vector or STING-WT-expressing cells (Fig. 3 A). We previously showed that *Sting*^{N153S/+} mice develop T cell cytopenia independent of IRF3 (Warner et al., 2017). STING-mediated IRF3 activation requires S366 residue (Liu et al., 2015). We thus further introduced S366A mutation to generate N154S/S366A double mutant to eliminate possible IRF3 activation by N154S. Similar to N154S, N154S/S366A expression also enhanced PMA+ionomycin-induced cell death (Fig. 3 A). The maximal extent of cell death observed in N154S/S366A cells is lower than that in N154S cells, suggesting a partial contribution of IRF3 in Jurkat T cell death in vitro. We also treated Jurkat cells expressing various STING mutants with CD3/CD28 antibodies, and again we observed increased cell death in N154S and N154S/S366A cells but not in STING-WT cells (Fig. S2, C and D). Together, these results suggest that the physiological level of STING-N154S expression intrinsically primes Jurkat T cells for apoptotic cell death when exposed to TCR signaling.

We next analyzed the relationship of TCR signaling, ER stress, and cell death. WT Jurkat T cells stimulated with PMA +ionomycin rapidly induced expression of UPR genes such as *GADD34*, *BIP*, and *CHOP* without activating cell death (Fig. S2 E). We next treated STING-WT or N154S Jurkat T cells with PMA +ionomycin. While STING-WT or N154S alone did not induce any UPR gene expression at baseline, N154S, but not STING-WT, significantly augmented expression of multiple UPR genes after PMA+ionomycin treatment (Fig. 3 B). We next pretreated STING-N154S cells with ER stress inhibitor TUDCA, which significantly reduced UPR gene expression in PMA+ionomycin-treated N154S cells (Fig. 3 C). TUDCA also prevented cell death in a dose-dependent manner in PMA+ionomycin-treated N154S cells as well as in N154S/S366A cells (Fig. 3, D and E). Another ER stress inducer thapsigargin (Tg) triggers ER calcium depletion, then ER stress. Combined Tg treatment and N154S or N154S/S366A expression, but not STING-WT expression, led to a drastic increase in cell death, suggesting a synergistic effect of ER stress and N154S expression in causing T cell death (Fig. 3 F and Fig. S2 F). Tg also induced N154S/S366A cell death in a dose-dependent manner, indicating that the synergistic effect is

independent of the STING-IRF3/IFN axis and dependent on the amount of ER stress (Fig. S2 G). These data suggest that TCR signaling induces ER stress but not immediate cell death; STING-N154S expression further augments ER stress, thus tipping the balance toward cell death.

Previous studies showed that small-molecule STING agonists such as 10-carboxymethyl-9-acridanone or DMXAA induce apoptosis in T cells (Gulen et al., 2017; Larkin et al., 2017). We next examined whether DMXAA can also synergize with TCR signaling in inducing T cell death. We treated primary mouse T cells with a high-dose DMXAA that causes substantially increased T cell death compared with mock when administered alone and a low-dose DMXAA that does not. When CD3/CD28 antibodies were combined with DMXAA to treat the T cells for 24 h, we indeed observed a synergistic effect only with the low-dose DMXAA condition (Fig. 3 G). This synergistic effect of DMXAA (low dose) with TCR signaling in causing T cell death was further augmented when we extended the DMXAA stimulation time up to 3 d (Fig. 3 H) and was dependent on Sting (Fig. 3 H). In concordance with this, combined treatment of DMXAA with CD3/CD28 antibody treatment (but not DMXAA alone) induced strong UPR gene expression (Fig. 3 I). These data suggest that extended suboptimal activation of STING by a ligand mimics gain-of-function mutation and both synergize with TCR signaling in causing ER stress and T cell death.

A novel STING motif and critical residues that regulate ER stress and the UPR

Based on our data thus far, we reasoned that STING-mediated ER stress and the UPR may be mediated through a novel motif distinct from the known TBK1-IRF3 binding domain required for IFN signaling. We used HEK293T cells that do not express detectable levels of endogenous cGAS or STING proteins (thus they are commonly used for STING functional domain-mapping studies). We cotransfected cGAS and STING into HEK293T cells to transiently activate STING signaling. Then, we measured IFN and UPR gene expression. cGAS and STING coexpression potently activated *IFNB* mRNA expression as expected. We also observed strong up-regulation of *ATF3* and *GADD34* mRNA expression, which are markers of ER stress and the UPR (Fig. 4 A).

We next used endogenous *GADD34* and *IFIT1* mRNA expression as main readouts for STING-mediated UPR and IFN response, respectively. STING contains a multi-pass transmembrane domain (TM) on the N terminus (required for ER localization), the CDN binding domain (CBD) in the middle (required for CDN binding), and the C-terminal tail (CTT) domain at the C terminus (required for TBK1 and IRF3 binding and activation of IFN signaling; see diagrams in Fig. 4 B). Deletion of TM, CBD, or CTT individually or in combination completely abolished STING-mediated IFN signaling as expected (Fig. 4 C and Fig. S3 A). In contrast, we found that CTT deletion (the TM-CBD construct or aa1-343) did not affect *GADD34* induction, suggesting that a distinct motif in TM-CBD is required for STING-mediated UPR (Fig. 4 C). STING-S366A mutant also blocked IFN signaling but remained active for inducing *GADD34* expression (Fig. 4 C), consistent with UPR being independent of

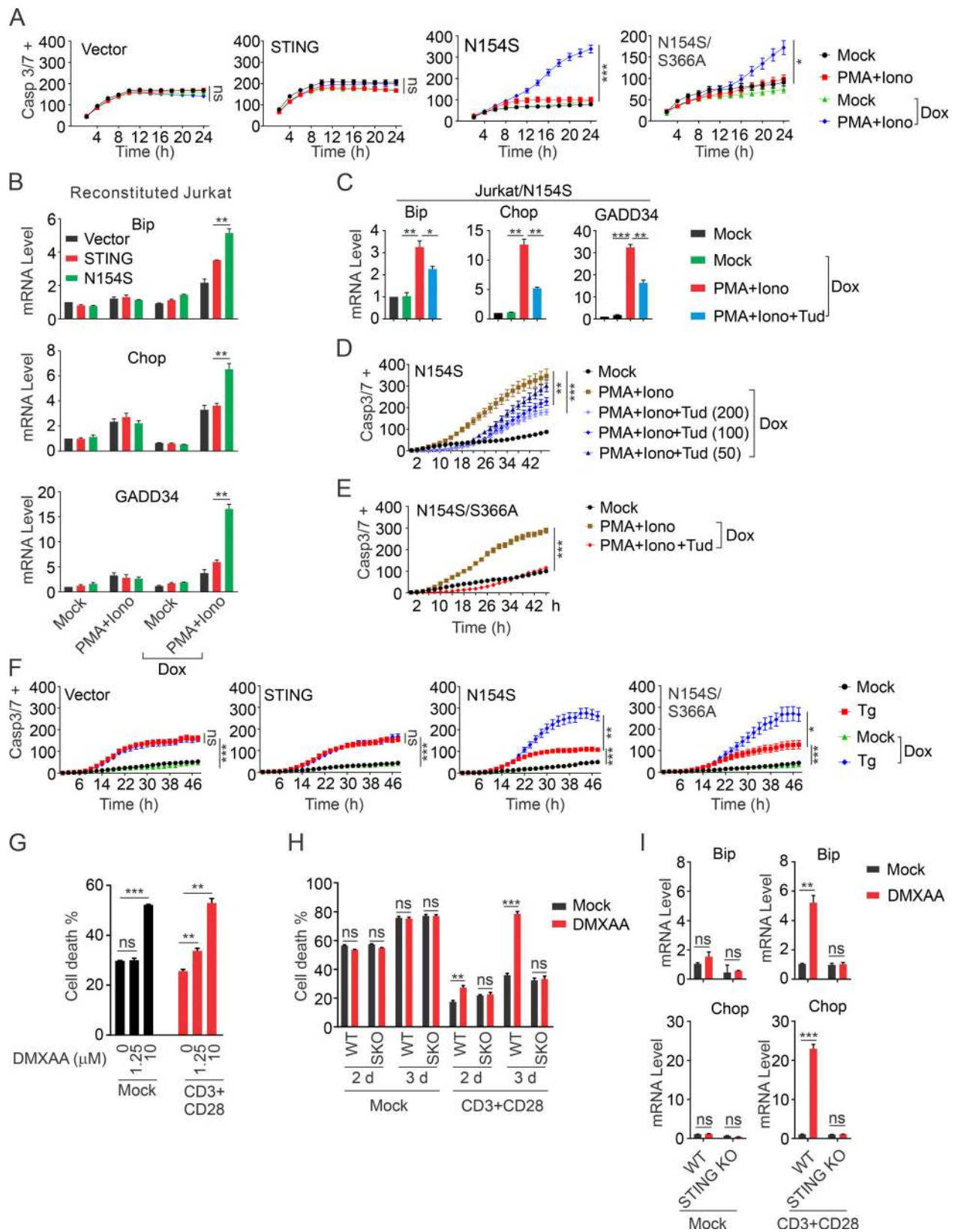


Figure 3. Human STING-N154S primes T cell death through ER stress. (A) Kinetics of cell death measured by IncuCyte. Reconstituted Jurkat T cells were mock or Dox treated for 1 d, then stimulated with or without PMA+ionomycin (PMA+Iono) for another day. Cell death kinetics was monitored using IncuCyte with a live-cell compatible caspase 3/7 dye (CellEvent Caspase-3/7; see Materials and methods). **(B and C)** qRT-PCR analysis of UPR gene expression in reconstituted Jurkat T cells. Experiments in B are Jurkat T cells reconstituted with Vector, WT STING, or N154S mutant (indicated as different color bars) that were either mock treated or treated with Dox alone, PMA+ionomycin alone, or Dox and PMA+ionomycin (indicated on bottom). Experiments in C are all N154S

cells, treated with indicated conditions on the right. UPR gene expression was measured by qRT-PCR. **(D)** Kinetics of cell death measured by InCuCyte in N154S cells. N154S cells were treated with Dox, PMA+ionomycin, and increasing doses of TUDCA (Tud; 50 μ M, 100 μ M, and 200 μ M). Cell death kinetics was monitored by InCuCyte as in A. **(E)** Kinetics of cell death measured by InCuCyte in N154S/S366A cells. N154S/S366A cells were treated with Dox and PMA+ionomycin with and without TUDCA (100 μ M). **(F)** InCuCyte analysis of reconstituted Jurkat T cells treated with Tg. Jurkat T cells reconstituted with indicated STING construct (top) were mock treated or treated with Tg (as indicated on the right). **(G and H)** T cell death analysis by annexin V staining and FACS analysis. Mouse primary T cells were stimulated for 1 d (G) or 2 d or 3 d (H) with mock or the indicated concentration of DMXAA in the presence or absence of CD3/CD28 antibodies. Both high-dose (10 μ M) and low-dose (1.25 μ M) DMXAA were analyzed at 1 d. Only low-dose DMXAA conditions were analyzed at 2 and 3 d. SKO, *Sting*^{-/-}. **(I)** qRT-PCR analysis of UPR gene expression in mouse primary T cells treated with DMXAA in the presence or absence of CD3/CD28 antibodies for 24 h. Error bars: SEM; *, $P < 0.05$; **, $P < 0.01$; ***, $P < 0.001$; ns, not significant. Student's *t* test. Data shown in all panels are representative of at least three independent experiments.

IRF3–IFN signaling axis as well as with our observations in reconstituted Jurkat cells.

Based on the crystal structure of STING C terminus (Zhang et al., 2013), the CBD contains the main CDN binding pocket plus an extra helix, aa322–343, that appears to be untethered to the rest of the structure on the exterior of the STING dimer (Fig. 4 D). This motif (helix aa322–343, called the “the UPR motif”) is also highly evolutionarily conserved, whereas the CTT is not (Fig. 4 D). We thus further trimmed off helix aa322–343 from the TM-CBD construct (1–343) to generate 1–322, which completely abrogated STING-mediated GADD34 induction (Fig. 4 E and Fig. S3 B). Internal deletion of helix aa322–343 in full-length STING (Δ 322–343) also abrogated STING-mediated GADD34 induction (Fig. 4 E).

It has been reported that the miniCTT motif (aa343–354) is required for STING-mediated inhibition of T cell proliferation through regulation of NF- κ B signaling (Cerboni et al., 2017). Due to the close proximity of the UPR motif (aa322–343) and the miniCTT motif (aa343–354), we next compared their roles in regulating UPR, IFN, and NF- κ B signaling. Internal deletion of the UPR motif (Δ 322–343) abrogated all three signaling pathways (Fig. 4 F). In contrast, internal deletion of the miniCTT motif (Δ 343–354) only abolished IFN signaling but did not affect STING-mediated UPR and NF- κ B signaling (Fig. 4 F and Fig. S3 C). Both the UPR motif and the miniCTT motif were essential for STING-N154S-induced NF- κ B signaling (ligand-independent activation), albeit weak overall, consistent with the previous report (Cerboni et al., 2017); when coexpressed with cGAS (ligand-dependent activation), only deletion of the UPR motif, but not deletion of the miniCTT motif, abolished NF- κ B activation (Fig. S3 D). Together, our results demonstrate that aa322–343 (the UPR motif) is essential for STING-mediated UPR and NF- κ B signaling activation in both a ligand-dependent and -independent manner.

To further pinpoint functional residues within the UPR motif and eliminate concerns of the deletion approach, we mutated two positive charged arginine residues that are exposed on the exterior surface of the STING dimer—thus, they are likely to be engaged in external interactions (Fig. 4 E). R331A/R334A (RRAA) had no effect on STING-mediated IFN response, while partially reduced GADD34 induction (Fig. 4 E). R331D/R334D (RRDD) completely abrogated STING-mediated GADD34 induction, with partial impact on IFN signaling (Fig. 4 E). To substantiate, we confirmed these mapping studies with another UPR target gene, *ATF3*, as readout. STING WT and TM-CBD are fully active for *ATF3* induction, whereas Δ 322–343 or RRDD mutation

completely abrogated *ATF3* induction (Fig. S3 E). In conclusion, these structural and functional analyses demonstrate that IFN and the UPR are mediated through distinct domains of STING, and that helix aa322–343, specifically residues R331 and R334, is critically required for STING-mediated UPR.

STING ER-to-Golgi translocation is critical for inducing ER stress and T cell death

To determine the role of the UPR motif in N154S-mediated T cell death, we next introduced RRDD mutations into the N154S construct and established a Jurkat T cell line with inducible expression of N154S/RRDD. N154S-mediated induction of UPR genes was completely abolished by further RRDD mutations after PMA+ionomycin treatment (Fig. 5 A). In InCuCyte experiments, N154S/RRDD expression also failed to enhance cell death after PMA+ionomycin or Tg treatment (Fig. 5 B). We next assessed STING WT and mutants' localization by stable expression in MEFs that allow more detailed subcellular microscopy. WT STING localizes to the ER, and N154S localizes to the ER-Golgi intermediate compartment then Golgi as expected (Dobbs et al., 2015). Interestingly, N154S/RRDD localizes to the ER similar to WT STING, suggesting that ER-to-Golgi translocation of N154S is critical for inducing ER stress and the UPR (Fig. 5 C). The ER calcium sensor STIM1 was recently shown to moonlight as an anchor for STING localization to the ER (Srikanth et al., 2019). STIM1 or its N-terminal STING-interacting domain inhibits STING-N154S trafficking and signaling. To corroborate with the N154S/RRDD finding, we ectopically expressed STIM1 (aa1–249) in Jurkat N154S cells to block STING trafficking, and we found that it also significantly reduced ER stress and cell death (Fig. 5 D). Together, these data demonstrate that the UPR motif of STING, specifically R331 and R334, is required for N154S ER-to-Golgi translocation, which is critical for activation of the UPR and T cell death.

STING-N154S disrupts ER calcium homeostasis

The increased sensitivity to Tg- and PMA/ionomycin-induced ER stress (both deplete the ER calcium store) prompted us to further investigate ER calcium homeostasis in N154S cells. Depletion of ER Ca²⁺ store activates Ca²⁺ influx across the plasma membrane (PM), a process known as store-operated Ca²⁺ entry, which maintains ER Ca²⁺ homeostasis and is essential for a wide array of cellular functions (Prakriya and Lewis, 2015). We used a live-cell microscopy technique with an intracellular calcium dye to monitor and quantify calcium flux in cells. We first treated Jurkat T cells expressing STING WT or mutants with Tg to

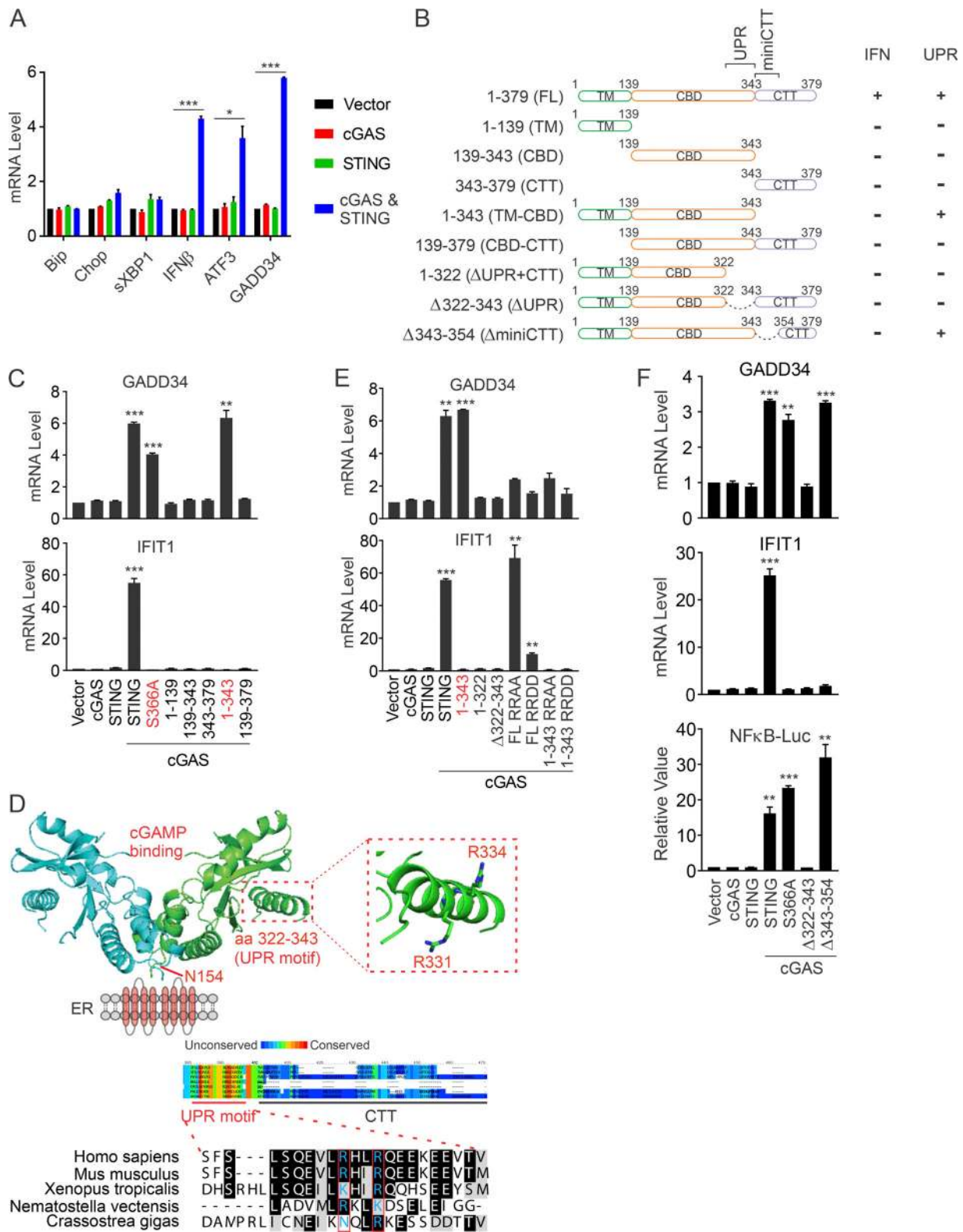


Figure 4. **A novel STING motif that regulates ER stress and the UPR.** (A) qRT-PCR analysis of UPR gene expression in HEK293T cells. HEK293T cells were transiently transfected with indicated cGAS or STING or both expressing plasmids. The *IFN β* - and UPR-related gene expression was measured by qRT-PCR 36 h after transfection. (B) Schematic diagrams of STING WT and truncation constructs and data summary. (C, E, and F) Structural and functional domain-mapping studies. HEK293T cells were transiently transfected with indicated plasmids (x axis). *GADD34*, *ATF3*, and *IFIT1* mRNA expressions were measured by qRT-PCR 36 h after transfection. (C) Truncation study of known STING domains. (E) Further fine mapping to define the UPR domain and critical residues in this region. FL, full length. (F) Comparison of the UPR motif versus the miniCTT motif by internal deletions. In the bottom panel of F, HEK293T cells were transfected with NF- κ B luciferase reporter and indicated expressing plasmid, and the luciferase activity was assayed 24 h after transfection. The P value was calculated by

comparing the indicated group with the vector control group. **(D)** The crystal structure of STING C terminus (4EF5) with key functional residues highlighted. Alignment of the UPR motif and CTT of STING homologs across different species are shown below. Error bars: SEM; *, $P < 0.05$; **, $P < 0.01$; ***, $P < 0.001$. Student's *t* test. Data shown are representative of at least three independent experiments.

deplete ER Ca^{2+} store and activate store-operated Ca^{2+} entry; then we added back Ca^{2+} in the medium to monitor Ca^{2+} flux across the PM (Liou et al., 2005). The first peak of fluorescent signals reflects release of ER Ca^{2+} into the cytosol following Tg treatment, whereas the second peak after Ca^{2+} add-back measures Ca^{2+} influx across the PM. Vector or STING-WT expression in Jurkat T cells did not affect either Ca^{2+} peak response (Fig. 6 A). In contrast, N154S significantly reduces both Tg-induced Ca^{2+} release from the ER as well as Ca^{2+} influx after add-back, indicating dysregulated calcium homeostasis (Fig. 6 A). Remarkably, N154S/RRDD restores calcium homeostasis to WT levels. Using primary T cells isolated from littermate WT and *Sting*^{N153S/+} mice, we again observed that *Sting*^{N153S/+} T cells exhibited defective ER Ca^{2+} release as well as influx compared with WT T cells (Fig. 6 B).

To further evaluate the relationship between ER Ca^{2+} signaling and ER stress and their respective synergy with STING-N154S, we compared Tg, which induces ER stress through depleting ER Ca^{2+} store and activating Ca^{2+} signaling, and tunicamycin (Tm), which induces ER stress through inhibiting N-linked glycosylation. We first confirmed their respective effect on Ca^{2+} signaling and ER stress. We used NFAT-Luc reporter as a readout for Ca^{2+} signaling (Zhang et al., 2016) and *Bip* and *Chop* mRNA expression as readouts for ER stress. Both Tg and Tm treatment activated ER stress, and only Tg, but not Tm, treatment activated Ca^{2+} signaling (Fig. 6, C and D). The Ca^{2+} signaling is specific because cyclosporine A (CsA, a calcineurin inhibitor) treatment abrogated Tg-induced Ca^{2+} signaling (Fig. 6 D). We next treated vector or N154S-expressing Jurkat T cells with mock, Tg, or increasing amounts of Tm and measured ER stress and cell death. Tm treatment induced significantly less cell death compared to Tg, despite incurring similar or more ER stress (Fig. 6, E and F). Our experiments thus far demonstrated that N154S synergizes strongly with TCR and Tg, which induce ER stress through calcium signaling. Together with the calcium flux defect observed in N154S cells, we conclude that dysregulated calcium signaling is the main contributing factor for N154S-mediated cell death.

The *OT-1* allele restores CD8⁺ T cells in *Sting*^{N153S/+} mouse

Our data thus far suggest that *Sting*-N153S renders T cells hyperresponsive to TCR signaling-induced ER stress, thus engaging the cell death pathway. We showed that inhibiting ER stress or caspases in vivo reduced T cell death (Fig. 2 E). Next, we wanted to test the role of TCR signaling in vivo. Both *Tcra* and *Tcrb* knockout mice are already severely deficient in T cells, making it difficult to rescue the T cell-deficient phenotype in *Sting*^{N153S/+} mice. A previous study showed that the *OT-1* allele can rescue T cell death associated with chronic ER stress in mice (Kamimura et al., 2015). Thus, we crossed *Sting*^{N153S/+} to the *OT-1* mouse that carry altered TCR locus in CD8⁺ T cells. We first analyzed ER stress markers in WT, *OT-1*, *Sting*^{N153S/+}, and

Sting^{N153S/+}*OT-1* splenic T cells by Western blot. While *Sting*^{N153S/+} T cells showed elevated expression of *Bip* and *Chop* compared with WT, *Sting*^{N153S/+}*OT-1* T cells reduced both UPR proteins to WT levels (Fig. 7 A). *Sting*^{N153S/+}*OT-1* CD8⁺ T cells completely abolished caspase activation and cell death compared with *Sting*^{N153S/+} CD8⁺ T cells (Fig. 7 B, Fig. S4 A, and Fig. S5 B). *Sting*^{N153S/+}*OT-1* also completely restored CD8⁺ T cell numbers in both spleen and peripheral blood (Fig. 7 C and Fig. S4 C). Other lymphoid and myeloid compartments such as CD45⁺ and CD19⁺ cells remain unaffected by *Sting*^{N153S/+} or *OT-1*. Interestingly, while CD3⁺ T cells are restored to WT levels in *Sting*^{N153S/+}*OT-1* mice, Ly6G⁺ myeloid cells remain significantly expanded compared with WT (Fig. S4 D). We did not observe any rescue of CD4⁺ T cells in *Sting*^{N153S/+}*OT-1* mice, because *OT-1* mice are also deficient in CD4⁺ T cells (Fig. 7 C and Fig. S5).

We also found that *Sting*^{N153S/+}*OT-1* T cells were fully switched to the naive state in contrast to the activated state of *Sting*^{N153S/+} T cells (Fig. 7 D). When treated with CD3/CD28 antibodies ex vivo, both *Sting*^{N153S/+} and *Sting*^{N153S/+}*OT-1* T cells failed to proliferate, while WT and *OT-1* T cells proliferated normally (Fig. 7 E). CD3/CD28 antibody treatment also triggered ER stress and cell death only in *Sting*^{N153S/+} and *Sting*^{N153S/+}*OT-1* T cells (Fig. 7, F and G). Taken together, our results demonstrated that altering CD8 TCR by crossing to the *OT-1* mice reduces ER stress and cell death signaling associated with *Sting*-N153S, thus restoring CD8⁺ T cells.

Restoring CD8⁺ T cells reduces inflammation and lung disease in the *Sting*^{N153S/+} mouse

Besides T cell cytopenia, SAVI patients also present with inflammation and lung disease, both of which are recapitulated in *Sting*^{N153S/+} mice (Warner et al., 2017). We therefore analyzed spleen, lung, and serum cytokines of WT, *OT-1*, *Sting*^{N153S/+}, and *Sting*^{N153S/+}*OT-1* mice. *Sting*^{N153S/+} mice have enlarged spleen, which was significantly reduced in size and splenocyte numbers in *Sting*^{N153S/+}*OT-1* mice (Fig. 8 A). Histopathological analysis of the lung showed that *Sting*^{N153S/+}*OT-1* mice have less severe perivascular inflammation in the lung compared with age-matched *Sting*^{N153S/+} mice (Fig. 8 B). We also observed that several inflammatory cytokines, such as IL-6, IL-2, IL-17, and RANTES, are significantly elevated in serum of *Sting*^{N153S/+} mice and reduced in serum of *Sting*^{N153S/+}*OT-1* mice (Fig. 8, C and D). These data demonstrate an important role for CD8⁺ T cells in *Sting*^{N153S/+} disease pathogenesis.

Discussion

In this study, we investigated the molecular mechanism by which STING-N154S mutation (N153S in mouse *Sting*) causes T cell death and revealed a novel function of STING in regulating calcium homeostasis and ER stress. To cause T cell death, STING-N154S synergizes with CD3/CD28,

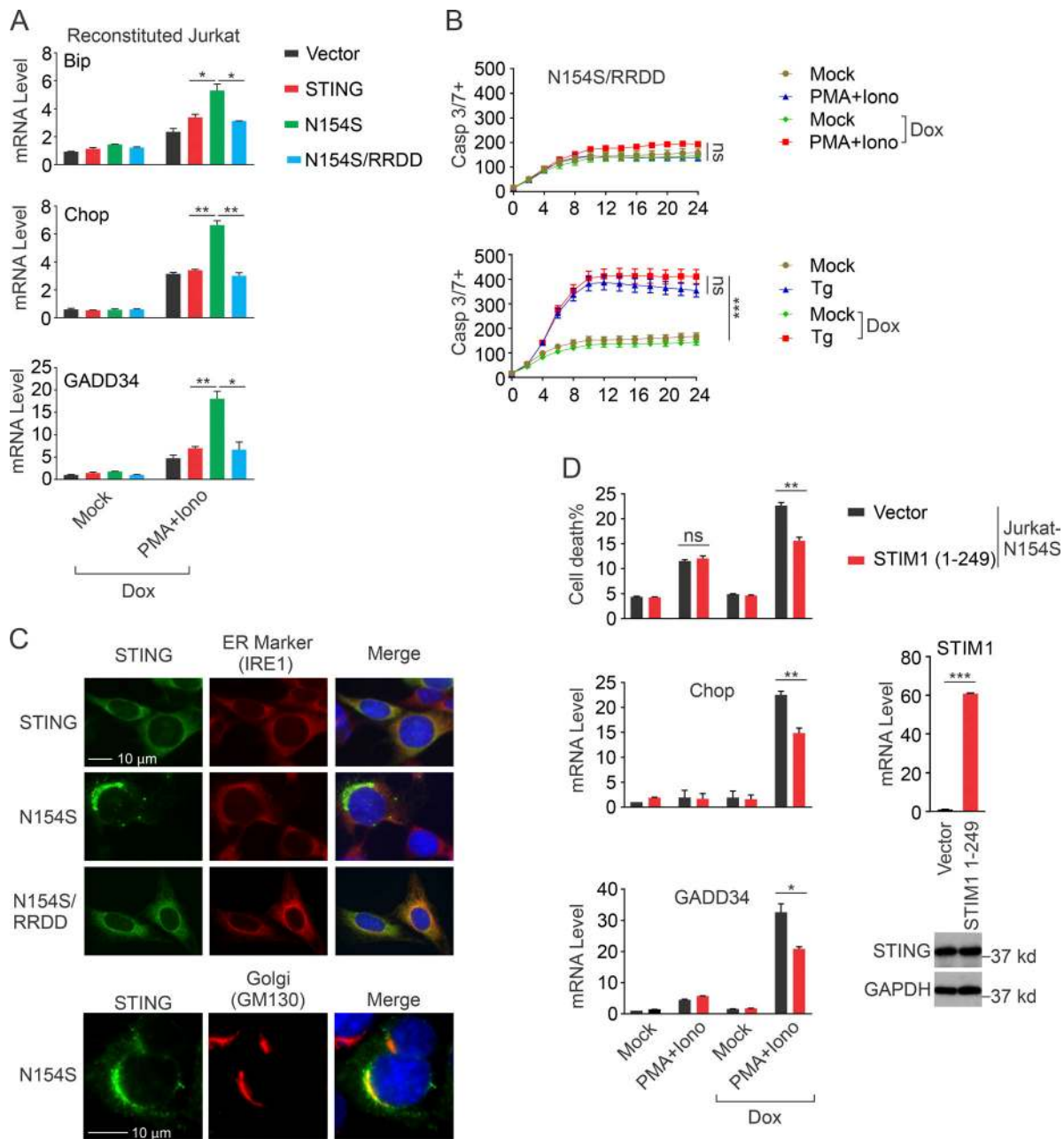


Figure 5. RRDD mutation abolishes STING-N154S-mediated ER-to-Golgi translocation, UPR, and T cell death. (A) qRT-PCR analysis of UPR gene expression in reconstituted Jurkat T cells. Jurkat T cells reconstituted with vector, STING, N154S, or N154S/RRDD were induced with Dox (0.5 μ g/ml) for 1 d, then stimulated with or without PMA (10 nM) + ionomycin (1 μ M; PMA+Iono) for another day. UPR gene expression was measured by qRT-PCR. (B) IncuCyte measurement of cell death kinetics in N154S/RRDD Jurkat cells. N154S/RRDD cells were treated with conditions indicated on the right, and cell death kinetics was measured by IncuCyte. (C) Fluorescent microscopy images of STING localization. *Sting*^{-/-} MEFs were stably transduced with a retroviral vector expressing WT STING or indicated mutant STING (N154S or N154S/RRDD). STING localization was detected by immunofluorescence staining of STING. IRE1 was costained as an ER marker and GM130 was costained as a Golgi marker. Bars, 10 μ m. (D) STIM1 (aa1–249) ectopic expression reduces ER stress and N154S Jurkat T cell death. N154S Jurkat T cells were reconstituted with empty vector or STIM1 (aa1–249). The cells were then mock treated or stimulated with PMA+ionomycin in the presence or absence of Dox. Cell death (top panel) was analyzed by annexin V staining. Expression of UPR genes (middle and bottom panels) was measured by qRT-PCR. STIM1 (aa1–249) expression is shown on the right. Error bars: SEM; *, $P < 0.05$; **, $P < 0.01$; ***, $P < 0.001$; ns, not significant. Student's *t* test. Data shown are representative of at least three independent experiments.

PMA+ionomycin, and Tg, which activate ER calcium signaling and ER stress, and to a lesser extent with Tm, which activates ER stress via a different route. STING-N154S also disrupts calcium homeostasis demonstrated by calcium flux imaging. Thus, our findings suggest that calcium signaling may be a

point of synergy in T cell death mediated by STING gain-of-function mutants. ER stress likely acts downstream as an important mediator for T cell death because we detected high expression of UPR proteins in *Sting*^{N153S/+} T cells and pharmacological inhibition of ER stress with the US Food and

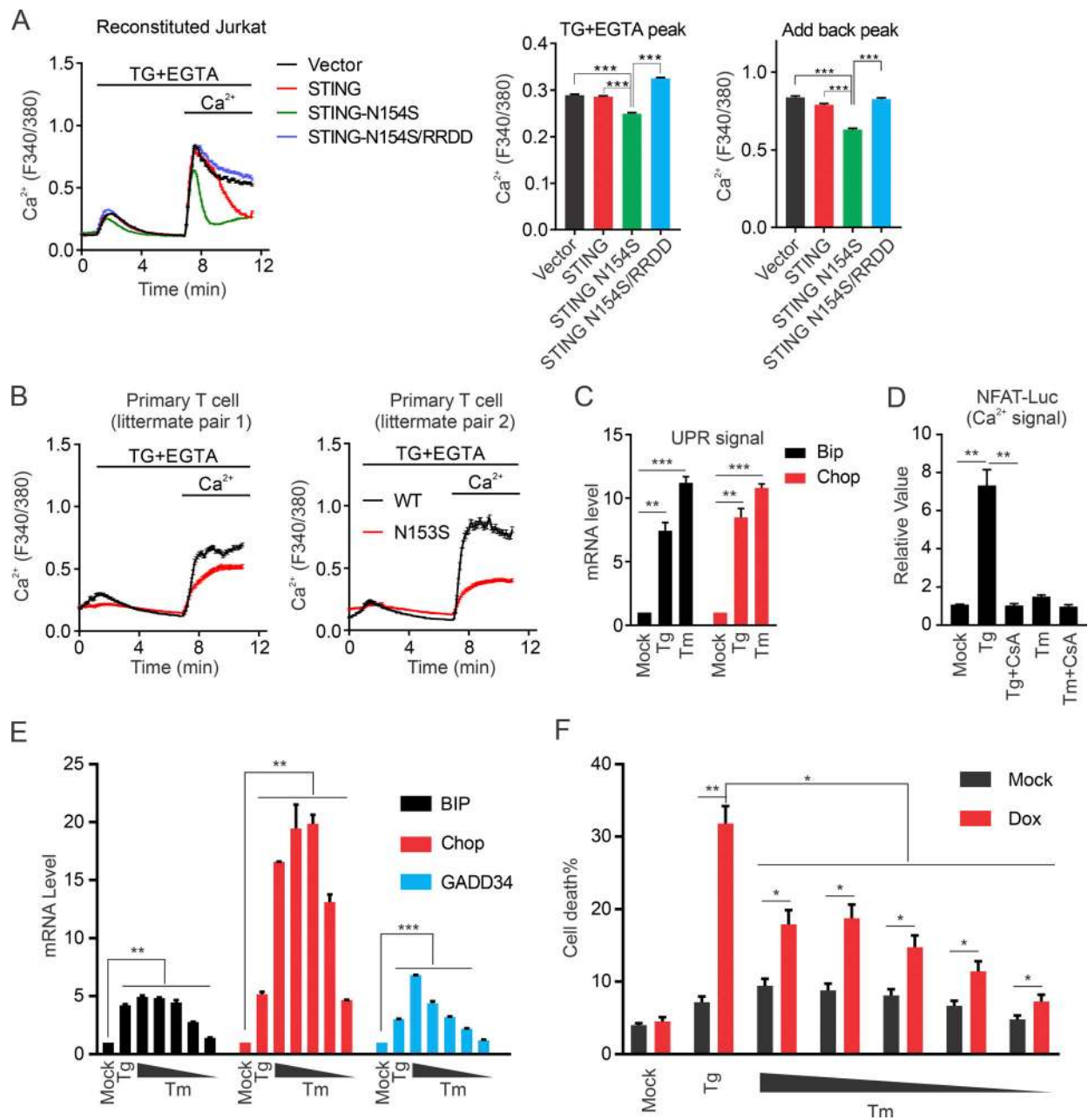


Figure 6. STING-N154S disrupts ER calcium homeostasis. (A) Relative changes in cytosolic Ca^{2+} concentration monitored by Fura-2 ratios in Jurkat T cells expressing indicated STING protein. Cells were stimulated with $1 \mu M$ Tg and 3 mM EGTA; 2 mM Ca^{2+} were added back 6 min after stimulation. Fura-2 intensities at 340-/380-nm excitation were recorded. Intensity ratios for Fura-2 are plotted. Curve graph (left) and bar graphs (right): mean with SEM (number of cells measured in each experiment was as follows: Vector, 580; STING, 589; STING-N154S, 633; STING-N154S/RRDD, 933). **(B)** Relative changes in cytosolic Ca^{2+} concentration in primary mouse T cells from two littermate pairs of WT and *Sting*^{N153S/+} mice. Cells were loaded with Fura2 and subjected to the same stimulation as in A. Fura-2 intensities at 340-/380-nm excitation were recorded. Intensity ratios for Fura-2 are plotted. Curve graphs: mean with SEM (number of cells measured in each experiment was as follows: WT-pair 1, 263; STING-N153S-pair 1, 194; WT-pair 2, 242; STING-N153S-pair 2, 271). Data are from a representative trace from two independent experiments. **(C)** qRT-PCR analysis of UPR gene expression in HEK293T cells treated with Tg or Tm for 16 h. **(D)** NFAT-Luc reporter assay in HEK293T cells treated with Tg or Tm. HEK293T cells were transfected with NFAT-Luc and TK-Renilla Luc (control) plasmids for 12 h, then treated with Tg or Tm with and without cyclosporine A (CsA). Dual-luciferase activity was measured 16 h after treatment. **(E and F)** UPR gene expression and cell death analysis of N154S Jurkat T cells treated with Tg or increasing concentrations of Tm. N154S Jurkat T cells were stimulated with fixed amount Tg (20 nM) and increasing concentrations of Tm (range, 0.0625–1 $\mu g/ml$). UPR gene expression was measured by qRT-PCR (E). Cell death was measured 48 h after treatment (F). Error bars: SEM; *, $P < 0.05$; **, $P < 0.01$; ***, $P < 0.005$. Student's *t* test. Data shown are representative of at least three independent experiments.

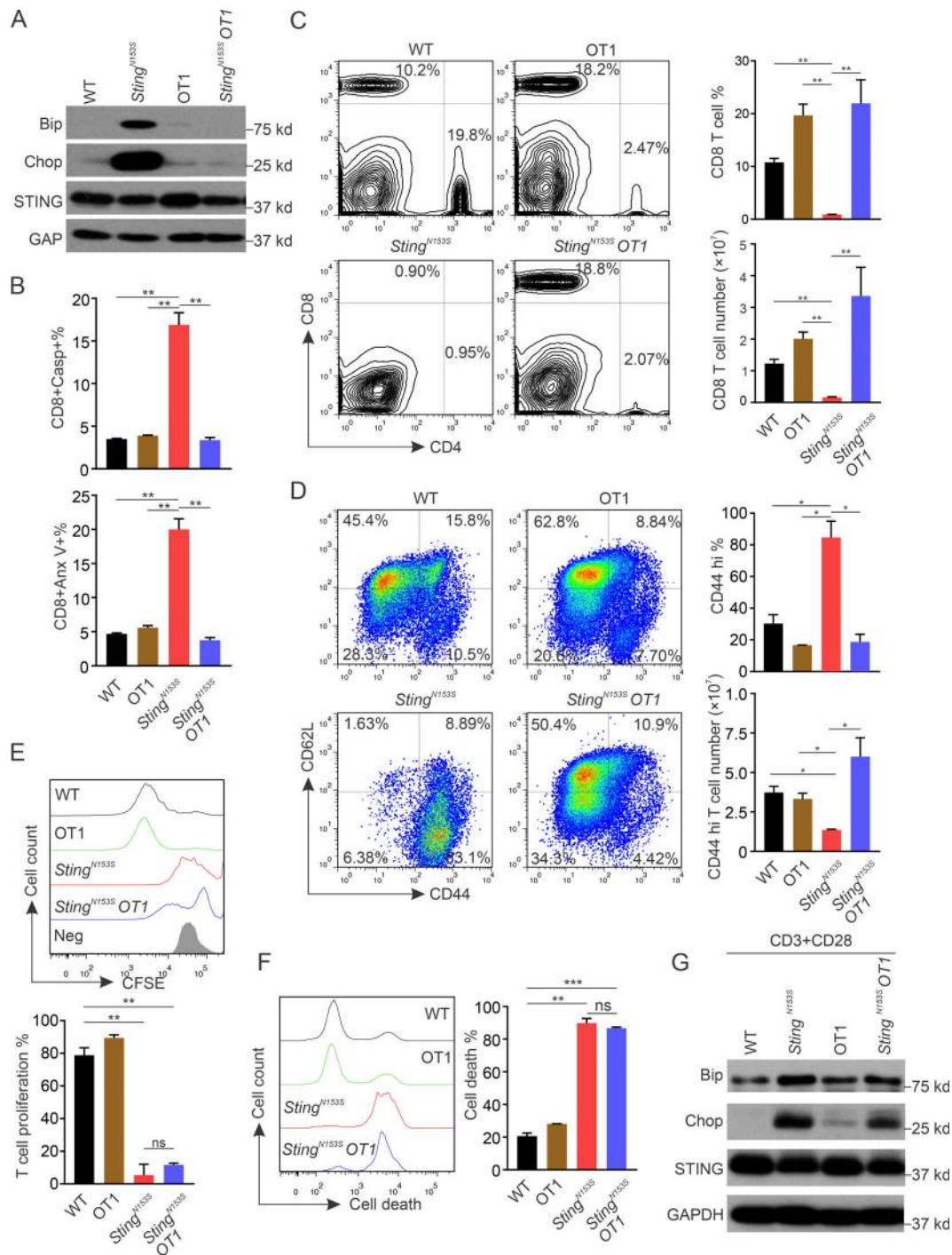


Figure 7. Altered TCR in *Sting*^{N153S/+} mice eliminates ER stress and T cell death. (A) Immunoblot of UPR proteins in fresh isolated T cells. The total T cells were isolated from the spleens of WT, *Sting*^{N153S}, *OT-1*, or *Sting*^{N153S}*OT-1* mice. UPR protein Bip and Chop were detected by Western blot. (B) FACS cell death analysis of CD8⁺ T cells from spleens of indicated mouse strains (bottom). Total splenocytes were stained for CD8 and cell death markers as in Fig. 1A. (C) T cell population analysis of indicated mouse strains. Total splenocytes isolated from the indicated mouse strains were stained for CD4 and CD8. Representative FACS plots are shown on the left, and CD8⁺ T cell percentages and cell numbers are summarized on the right. (D) T cell activation analysis of indicated mouse strains. Total splenocytes isolated from indicated mouse strains were stained for CD8, CD44, and CD62L. Representative FACS plots are shown on the left, and CD44^{hi} (antigen experienced or activated) in the CD8⁺ population are summarized on the right. (E) T cell proliferation analysis of indicated mouse strains. Total splenocytes were isolated from indicated mouse strains and stained with the CFSE dye. Then, cells were stimulated with CD3/CD28 antibodies for 3 d. CFSE dilution in the CD8⁺ T cell population was analyzed by FACS. A representative set of CFSE dilution plots is shown on the top, and summarized data from *n* = 4 mice per genotype are shown on the bottom. (F) T cell death analysis of indicated mouse strains. Total splenocytes from indicated mouse strains were stimulated with CD3/CD28 antibodies ex vivo for 3 d. Cells were then stained for CD8 and cell death markers and analyzed by FACS. A representative set of FACS plots is shown on the left, and summarized data from *n* = 4 mice per genotype are shown on the right. (G) Immunoblot of UPR proteins in indicated mouse T cells after CD3/CD28 antibody stimulation. Total T cells were isolated from spleens of indicated mouse strains, then stimulated with CD3/CD28 antibodies for 1 d. UPR proteins were detected by Western blot. Error bars: SEM; *, *P* < 0.05; **, *P* < 0.01; ***, *P* < 0.001. Student's *t* test. Anx V, annexin V; Casp, caspase.

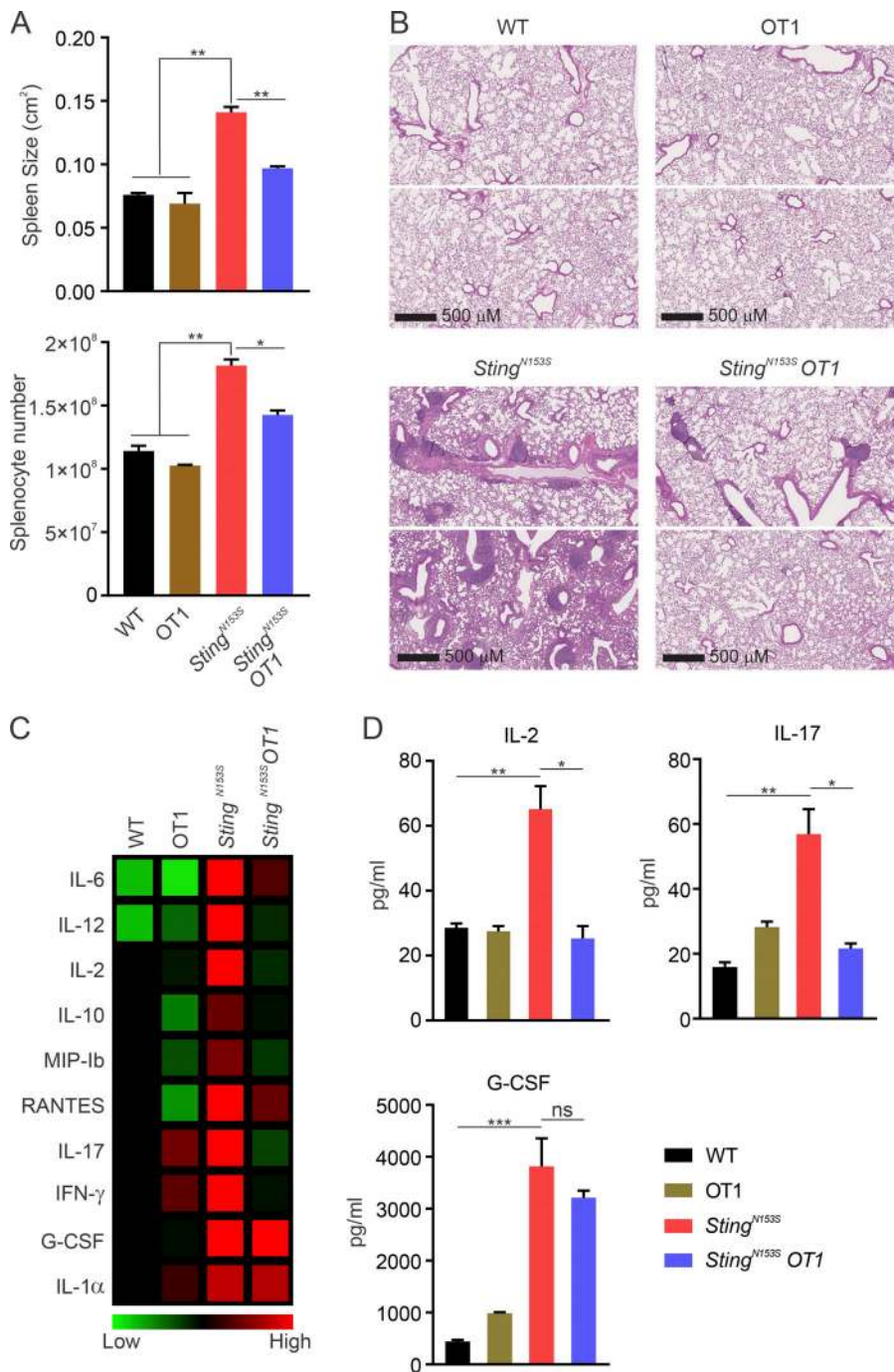


Figure 8. Restoration of CD8⁺ T cells relieves inflammation and lung disease. (A) Spleen size and total splenocyte number of indicated mouse strains. (B) Histopathological analysis of the lung from indicated mouse strains. H&E images of paraffin-embedded lung sections from 3-mo and sex-matched WT littermate, *Sting*^{N153S}, OT-1, and *Sting*^{N153S} OT-1 mice. *n* = 4. Bars, 500 μm. (C and D) Multiplex cytokine analysis of serum from indicated mouse strains. The overall cytokine comparison is shown in the heat map (C), and the representative cytokine concentrations are shown on the bar graphs (D). *n* = 4. Error bars: SEM; *, *P* < 0.05; **, *P* < 0.01; ***, *P* < 0.001; ns, not significant. Student's *t* test.

Drug Administration–approved compound TUDCA prevented *Sting*^{N153S/+} T cell death in vitro and in vivo.

We also observed rescue of CD8⁺ T cells as well as amelioration of spontaneous lung disease by crossing *Sting*^{N153S/+} to the OT-1 mouse. Given the complexity of altered TCR repertoire and homeostatic self-MHC antigen experience associated with the OT-1 allele, we do not know the exact cause of the rescue. We observed that *Sting*^{N153S/+} T cells are activated, which could be a result of T cell proliferation in an empty compartment due to lymphopenia or, alternatively, homeostatic reactivity to self-MHC-I antigens (Kieper and Jameson, 1999). One possible explanation for the OT-1 rescue could be that OT-1 somehow

reduced the threshold of self-peptide MHC reactivity of *Sting*^{N153S/+} T cells, thus reducing activation and synergistic effect with N153S. Nonetheless, these data demonstrate an important role for CD8⁺ T cells and possibly TCR signaling in *Sting*^{N153S/+} disease pathogenesis.

Molecularly, we showed that STING activates ER stress and the UPR through a novel motif located in the helix aa322–343 that we name “the UPR motif.” The UPR motif is evolutionarily conserved in most animal phyla and is distinct from the previously characterized CTT domain (required for IFN signaling) or the miniCTT. We also pinpointed two highly conserved residues, R331 and R334, as critical residues for STING-mediated UPR, and

point mutations of these two residues abolished the UPR and prevented cell death induced by STING-N154S expression in Jurkat T cells.

Our data also reveal a curious function of STING on maintaining calcium homeostasis, which appears to require the UPR motif and proper localization of STING on the ER. Acute stimulation of mouse cells with STING agonist triggers a rapid increase in intracellular calcium (Kim et al., 2017). We showed here that low-dose DMAXX stimulation also primes WT T cells for cell death after CD3/CD28 treatment, mimicking gain-of-function mutant phenotypes. These observations collectively bring out a unified model in which STING activation, either ligand dependent or independent, triggers ER-to-Golgi translocation that somehow disrupts ER calcium homeostasis. An important addition to this model comes from a recent study showing that the ER calcium sensor STIM1 moonlights as an ER anchor for STING (Srikanth et al., 2019). We ectopically expressed the STING-anchoring domain of STIM1 (aa1–249) and found that it reduced ER stress and cell death in N154S cells. Whether STING directly regulates ER calcium homeostasis or through STIM1 or other components of the calcium signaling pathway requires further study.

The cGAS-STING pathway has been shown to regulate cellular senescence and cell death through the production of senescence-associated secretory phenotype factors and partially the p53 pathway (Glück et al., 2017; Gulen et al., 2017; Yang et al., 2017). Our findings revealed that chronic activation of STING gain-of-function mutants do not cause T cell death directly in vivo (e.g., *Sting*^{N153S/+}*OT-1*); rather, these mutants chronically elevate ER stress and the UPR through disrupting calcium homeostasis that intrinsically primes T cells to become hyperresponsive to TCR signaling, thus tipping the balance toward committing cell death. We demonstrated this in the physiological disease setting in vivo and defined the molecular functional domain in vitro. Importantly, restoring at least the CD8⁺ T cells can largely restore tissue homeostasis of the spleen and the lung. Therefore, from the therapeutic standpoint, ER stress and the UPR are exciting molecular targets and T cells are novel cellular targets for treating STING-associated diseases such as SAVI. Several ER stress inhibitors are US Food and Drug Administration-approved drugs with an excellent safety profile; thus, they should be considered as therapy for SAVI.

Materials and methods

Mice and cells

The *Sting*^{N153S/+} mice were generated and described previously (Warner et al., 2017). *OT-1* mice were obtained from the Jackson Laboratory. All mice were maintained in pathogen-free barrier facilities and were used in accordance with protocols approved by the Institutional Animal Care and Use Committee at University of Texas Southwestern Medical Center. For mouse treatment with inhibitors, sex- and age-matched *Sting*^{N153S/+} mice were i.p. injected with PBS or TUDCA (250 mg/kg) or QVDOPH (10 mg/kg) three times per wk. After 14 d of treatment, mice from different treatment group were bled, and T cells from blood were analyzed by FACS. HEK293T, MEFs, and human

fibroblasts were maintained in DMEM with 10% (vol/vol) FBS, 2 mM L-glutamine, 10 mM HEPES, and 1 mM sodium pyruvate (complete DMEM) with the addition of 100 U/ml penicillin and 100 mg/ml streptomycin and cultured at 37°C with 5% CO₂. Jurkat T cells were maintained in Roswell Park Memorial Institute (RPMI) medium with 10% FBS and supplement.

Antibodies

The following antibodies were used for flow cytometry: anti-CD8α (53–6.7), anti-CD4 (L3T4), anti-CD3ε (145-2C11), anti-CD25 (PC61.5), anti-CD69 (H1.2F3), anti-CD44 (IM7), anti-CD62L (MEL-14), CD19 (1D3), CD45 (30-F11), and Ly6G (1A8) all from BD Biosciences or BioLegend. The splenocytes were stained with the indicated panel of antibodies according to the manufacturers' instructions, and then analyzed by BD FACSCalibur or BD LSR II FACs machines. Purified anti-CD3ε (145-2C11) and anti-CD28 (37.51; both from eBioscience) were used at the appropriate concentration for T cell activation. The following antibodies were used for immunoblotting analysis: anti-STING (D2P2F; Cell Signaling), anti-TBK1 (D1B4; Cell Signaling), anti-pTBK1 (D52C2; Cell Signaling), anti-IRF3 (D83B9, Cell Signaling), anti-pIRF3 (4D4G, Cell Signaling), anti-cleaved PARP (D64E10; Cell Signaling), anti-cleaved caspase 3 (5A1E; Cell Signaling), anti-Bip (C50B12; Cell Signaling), anti-Chop (L63F7; Cell Signaling), anti-eIF2α (D7D3; Cell Signaling), and anti-p-eIF2α (119A11; Cell Signaling).

Plasmids

The STING constructs in MRX retrovirus vector was described previously (Dobbs et al., 2015). The human STING was cloned into the PCMV-3Tag-1b as described previously (Wu et al., 2015). The different truncations were cloned into the same vector with the primers listed in Table S1. The point mutants of STING were made using the Quikchange II Site-Directed Mutagenesis Kit (Agilent Technologies, Inc.). The STING WT and mutants were amplified with Flag tag from the respective PCMV constructs, and then subcloned into the pEasiv vector (Wu et al., 2015) by Gibson assembly (New England Biolabs). Human STIM1 1–249 was amplified from cDNA and subcloned into the pEasiv vector. NFκB-Luc and pRL-TK were a gift from Dr. Fanxiu Zhu (Florida State University, Tallahassee, FL). NFAT-Luc was purchased from Addgene.

In vitro T cell proliferation assay and cell death assay

Splenocytes were labeled with carboxyfluorescein diacetate succinimidyl ester (CFSE; Thermo Fisher Scientific; C34554) according to the manufacturer's instructions. The labeled cells were plated in 24-well plates coated with anti-CD3ε (10 μg/ml; 145-2C11; eBioscience) and anti-CD28 (10 μg/ml; 37.51; eBioscience) for 3 d. The cells were then collected and stained with anti-CD4 or anti-CD8 antibody for different T cell subpopulation analysis. The cell proliferation was dictated by CFSE dilution. For primary T cell death analysis, the fresh isolated splenocytes were first stained with anti-CD3, anti-CD4, or anti-CD8 antibodies to distinguish different T cell populations, and then stained with cell death marker annexin V (BioLegend) or CaspACE FITC-VAD-FMK (Promega) according to the

manufacturers' instructions. Cell death was examined by FACS using BD FACSCalibur or BD LSR II flow cytometry. The DMXAA-induced T cell death experiment was performed as follows. The mouse CD4⁺ T was isolated from spleen with the CD4⁺ T Cell Isolation Kit (Miltenyi Biotec; 130-104-454) according to the manufacturer's instructions. T cells were then stimulated with the indicated dose of DMXAA in the presence or absence of anti-CD3 and anti-CD28 antibodies. Cells were then stained with annexin V and analyzed by FACS. Alternatively, cells were analyzed for ER stress gene expression by quantitative PCR (qPCR) 24 h after treatment.

Jurkat T cell reconstitution and IncuCyte cell death assay

The human STING WT, STING N154S, STING N154S/S366A, and STING N154S/RRDD were cloned into the pEasily lentiviral vector with N-terminal FLAG tag. The lentivirus production and transduction were described previously (Wu et al., 2015). Briefly, the lentivirus was produced in HEK293T cells by cotransfection of pEasily, p8.91, and pMD2.G at a ratio of 1:1:0.5. The lentivirus was harvested and filtered to remove cell debris at 2 d after transfection. The virus was further concentrated with Lenti-X concentrator (Clontech). The Jurkat cells were transduced with high multiplicity of infection lentivirus with spin infection at 800 *g* for 1 h at room temperature. We usually achieve close to 100% transduction efficiency confirmed by E2-Crimson fluorescence marker expression. For the STING N154S cells, we further sorted out the N154 high- and low-expression population by flow cytometry (FACSCalibur; BD Biosciences). The Jurkat STING N154S cells were transiently induced with Dox (0.5 μg/ml) for 12 h; the E2-Crimson-positive cells were sorted into two populations, E2-Crimson high expression and low expression, which represent N154S high- and low-expressing cells, respectively. The Jurkat-N154S (low-expression) cells were further transduced with human STIM1 (1–249 aa)-expressing lentivirus to establish the Jurkat-N154S/STIM1 (1–249 aa) cell line. The cells were cultured in complete RPMI medium for 1 wk and then used for the experiment. For cell death experiments, the reconstituted Jurkat cells were induced with Dox (0.5 μg/ml) for 3 d, and then stained with annexin V for cell death analysis by FACS. Alternatively, the cells were induced with Dox for 1 d, then stimulated with PMA (10 nM) plus ionomycin (1 μM) or the indicated concentration of Tg for another day. The cells were stained with annexin V for cell death analysis. To monitor the cell death kinetics by IncuCyte S3 Live-Cell Analysis System (Sartorius), the cells were prestained with CellEvent Caspase-3/7 probe (Thermo Fisher Scientific; R37111), then induced with or without Dox (0.5 μg/ml) in the presence or absence of PMA (10 nM) plus ionomycin (1 μM), or Tg (50 nM) in clear-bottom 96-well plates. All wells were continuously monitored with a 10× objective that images multiple locations of each well every 2 h. Images were analyzed using the cell death software module in IncuCyte.

RNA isolation and qRT-PCR

Total RNA was isolated with TRI reagent according to the manufacturer's instructions (Sigma-Aldrich). cDNA was synthesized with an iScript cDNA synthesis kit (Bio-Rad). ITaq

Universal SYBR Green Supermix (Bio-Rad) and an CFX96 Touch Real-Time PCR Detection System (Bio-Rad) were used for qRT-PCR analysis (primer sequences listed in Table S2). Hprt and Gapdh were used as housekeeping genes for data normalization.

Histopathological analysis of the mouse lung

Lung tissue H&E staining was performed as previously described (Warner et al., 2017). Briefly, tissue was isolated and fixed in 4% paraformaldehyde for 24 h at 4°C and resuspended in 70% ethanol before being embedded in paraffin blocks. Tissue sections were subjected to H&E staining. Samples were imaged using a slide scanner Hamamatsu Nanozoomer and viewed with Hamamatsu NDPview2 software.

Luciferase reporter assays

HEK293T cells seeded on 24-well plates were transiently transfected with 100 ng of the NF-κB luciferase reporter plasmid together with a total of 300 ng of various expression plasmids and/or empty vector controls using Lipofectamine 2000. As an internal control, 10 ng of pRL-TK (Renilla luciferase) was transfected simultaneously. For the Tg-induced Ca²⁺ signaling, NFAT-Luc (100 ng) and pRL-TK (10 ng) were transfected into HEK293T cells for 12 h, then stimulated with Tg overnight. Luciferase assays were then performed at 24 h after transfection according to the Promega Dual-Luciferase Reporter Assay System protocol. The relative luciferase activity was expressed as arbitrary units by normalizing firefly to Renilla luciferase activity.

Cytosolic Ca²⁺ level measurements

For measuring cytosolic Ca²⁺ levels, the reconstituted Jurkat cells or primary T cells were loaded with 1 μM Fura-2-acetoxymethyl ester in extracellular buffer (ECB) containing 0.05% pluronic F-127 and 0.1% BSA for 30 min at room temperature, avoiding light. Loaded cells were then washed with ECB containing 0.1% BSA and incubated in ECB for another 15–30 min before the experiments. Single-cell Ca²⁺ images were taken with a 10× objective or 20× objective and an automated microscope custom built on an Eclipse Ti microscope with a camera (HQ2; Photometrics). The microscope was controlled by Micro-Manager software (Chang et al., 2018). Intracellular Ca²⁺ levels were indicated by ratio of 510-nm emission excited at 340 nm over those at 380 nm.

Cytokine array

Cytokine array was performed as previously described (Warner et al., 2017). Briefly, cohort mouse serum was collected and analyzed using the Bio-Plex Pro Mouse Cytokine Group I Panel 23-Plex Assay kit (Bio-Rad). The BioPlex Pro Assay was performed by the University of Texas Southwestern Genomics and Microarray Core according to the manufacturer's protocol.

Statistical analysis

Data are presented as the mean ± SEM. The statistical significance of differences was determined by Student's *t* test. Statistical tests performed are indicated in figure legends (*, *P* < 0.05; **, *P* < 0.01; ***, *P* < 0.001).

Online supplemental material

Fig. S1 shows chronic activation of ER stress and the UPR in the *Sting*^{N153S/+} mouse. Fig. S2 shows reconstitution of STING-N154S-mediated T cell death in human Jurkat T cells. Fig. S3 shows mapping of the critical motif and residues for STING-mediated UPR; Fig. S4 shows the *OT-1* rescues CD8⁺ T cells in *Sting*^{N153S/+} mice. Fig. S5 shows that CD4⁺ T cells are not rescued by *OT-1* in *Sting*^{N153S/+} mice. Table S1 lists cloning primers, and Table S2 lists qPCR primers.

Acknowledgments

We thank R. Goldbach-Mansky (National Institute of Allergy and Infectious Diseases, Bethesda, MD) for SAVI patient fibroblasts and R. Huang and R. Maple for help with maintaining *Sting*^{N153S/+} mice. We thank members of the Yan laboratory for helpful discussions.

This work is supported by National Institutes of Health grants AR067135 and AI134877 (N. Yan), GM113079 (J. Liou), and AR070918 (J.J. Miner); Cancer Prevention and Research Institute of Texas grant RP180288 (N. Yan); and the Burroughs Wellcome Fund (N. Yan).

The authors declare no competing financial interests.

Author contributions: J. Wu performed most of the experiments. Y.-J. Chen and J. Liou helped with performing the calcium experiments and data analysis. T. Sakai and N. Dobbs helped with mouse experiments. J.J. Miner provided advice, edited the final version of the manuscript, and provided *Sting*^{N153S/+} mice. J. Wu and N. Yan analyzed the data and wrote the paper.

Submitted: 27 November 2018

Revised: 29 January 2019

Accepted: 25 February 2019

References

- Bouis, D., P. Kirstetter, F. Arbogast, D. Lamon, V. Delgado, S. Jung, C. Ebel, H. Jacobs, A.-M. Knapp, N. Jeremiah, et al. 2018. Severe combined immunodeficiency in *Sting* V154M/WT mice. *J. Allergy Clin. Immunol.* 143: 712–725.e5. <https://doi.org/10.1016/j.jaci.2018.04.034>
- Burdette, D.L., K.M. Monroe, K. Sotelo-Troha, J.S. Iwig, B. Eckert, M. Hyodo, Y. Hayakawa, and R.E. Vance. 2011. STING is a direct innate immune sensor of cyclic di-GMP. *Nature.* 478:515–518. <https://doi.org/10.1038/nature10429>
- Carboni, S., N. Jeremiah, M. Gentili, U. Gehrmann, C. Conrad, M.-C. Stolzenberg, C. Picard, B. Neven, A. Fischer, S. Amigorena, et al. 2017. Intrinsic antiproliferative activity of the innate sensor STING in T lymphocytes. *J. Exp. Med.* 214:1769–1785. <https://doi.org/10.1084/jem.20161674>
- Chang, C.-L., Y.-J. Chen, C.G. Quintanilla, T.-S. Hsieh, and J. Liou. 2018. EBI binding restricts STIM1 translocation to ER-PM junctions and regulates store-operated Ca²⁺ entry. *J. Cell Biol.* 217:2047–2058. <https://doi.org/10.1083/jcb.201711151>
- Dobbs, N., N. Burnaevskiy, D. Chen, V.K. Gonugunta, N.M. Alto, and N. Yan. 2015. STING activation by translocation from the ER is associated with infection and autoinflammatory disease. *Cell Host Microbe.* 18:157–168. <https://doi.org/10.1016/j.chom.2015.07.001>
- Gao, D., J. Wu, Y.-T. Wu, F. Du, C. Aroh, N. Yan, L. Sun, and Z.J. Chen. 2013. Cyclic GMP-AMP synthase is an innate immune sensor of HIV and other retroviruses. *Science.* 341:903–906. <https://doi.org/10.1126/science.1240933>
- Glück, S., B. Guey, M.F. Gulen, K. Wolter, T.-W. Kang, N.A. Schmacke, A. Bridgeman, J. Rehwinkel, L. Zender, and A. Ablasser. 2017. Innate

- immune sensing of cytosolic chromatin fragments through cGAS promotes senescence. *Nat. Cell Biol.* 19:1061–1070. <https://doi.org/10.1038/ncb3586>
- Gulen, M.F., U. Koch, S.M. Haag, F. Schuler, L. Apetoh, A. Villunger, F. Radtke, and A. Ablasser. 2017. Signalling strength determines proapoptotic functions of STING. *Nat. Commun.* 8:427. <https://doi.org/10.1038/s41467-017-00573-w>
- Jeremiah, N., B. Neven, M. Gentili, I. Callebaut, S. Maschalidi, M.-C. Stolzenberg, N. Goudin, M.-L. Frémond, P. Nitschke, T.J. Molina, et al. 2014. Inherited STING-activating mutation underlies a familial inflammatory syndrome with lupus-like manifestations. *J. Clin. Invest.* 124:5516–5520. <https://doi.org/10.1172/JCI79100>
- Kamimura, D., K. Katsunuma, Y. Arima, T. Atsumi, J.-J. Jiang, H. Bando, J. Meng, L. Sabharwal, A. Stofkova, N. Nishikawa, et al. 2015. KDEL receptor 1 regulates T-cell homeostasis via PPI that is a key phosphatase for ISR. *Nat. Commun.* 6:7474. <https://doi.org/10.1038/ncomms8474>
- Kieper, W.C., and S.C. Jameson. 1999. Homeostatic expansion and phenotypic conversion of naïve T cells in response to self peptide/MHC ligands. *Proc. Natl. Acad. Sci. USA.* 96:13306–13311. <https://doi.org/10.1073/pnas.96.23.13306>
- Kim, S., P. Koch, L. Li, L. Peshkin, and T.J. Mitchison. 2017. Evidence for a role of calcium in STING signaling. *bioRxiv.* <https://doi.org/10.1101/145854>
- König, N., C. Fiehn, C. Wolf, M. Schuster, E. Cura Costa, V. Tüngler, H.A. Alvarez, O. Chara, K. Engel, R. Goldbach-Mansky, et al. 2017. Familial chilblain lupus due to a gain-of-function mutation in STING. *Ann. Rheum. Dis.* 76:468–472. <https://doi.org/10.1136/annrheumdis-2016-209841>
- Larkin, B., V. Ilyukha, M. Sorokin, A. Buzdin, E. Vannier, and A. Poltorak. 2017. Cutting Edge: Activation of STING in T Cells Induces Type I IFN Responses and Cell Death. *J. Immunol.* 199:397–402. <https://doi.org/10.4049/jimmunol.1601999>
- Liou, J., M.L. Kim, W.D. Heo, J.T. Jones, J.W. Myers, J.E. Ferrell Jr., and T. Meyer. 2005. STIM is a Ca²⁺ sensor essential for Ca²⁺-store-depletion-triggered Ca²⁺ influx. *Curr. Biol.* 15:1235–1241. <https://doi.org/10.1016/j.cub.2005.05.055>
- Liu, S., X. Cai, J. Wu, Q. Cong, X. Chen, T. Li, F. Du, J. Ren, Y.-T. Wu, N.V. Grishin, and Z.J. Chen. 2015. Phosphorylation of innate immune adaptor proteins MAVS, STING, and TRIF induces IRF3 activation. *Science.* 347:aaa2630. <https://doi.org/10.1126/science.aaa2630>
- Liu, Y., A.A. Jesus, B. Marrero, D. Yang, S.E. Ramsey, G.A.M. Sanchez, K. Tenbrock, H. Wittkowski, O.Y. Jones, H.S. Kuehn, et al. 2014. Activated STING in a vascular and pulmonary syndrome. *N. Engl. J. Med.* 371: 507–518. <https://doi.org/10.1056/NEJMoa1312625>
- Margolis, S.R., S.C. Wilson, and R.E. Vance. 2017. Evolutionary Origins of cGAS-STING Signaling. *Trends Immunol.* 38:733–743. <https://doi.org/10.1016/j.it.2017.03.004>
- Melki, I., Y. Rose, C. Ugenti, L. Van Eyck, M.-L. Frémond, N. Kitabayashi, G.I. Rice, E.M. Jenkinson, A. Boulai, N. Jeremiah, et al. 2017. Disease-associated mutations identify a novel region in human STING necessary for the control of type I interferon signaling. *J. Allergy Clin. Immunol.* 140:543–552.e5. <https://doi.org/10.1016/j.jaci.2016.10.031>
- Pino, S.C., B. O'Sullivan-Murphy, E.A. Lidstone, T.B. Thornley, A. Jurczyk, F. Urano, D.L. Greiner, J.P. Mordes, A.A. Rossini, and R. Bortell. 2008. Protein kinase C signaling during T cell activation induces the endoplasmic reticulum stress response. *Cell Stress Chaperones.* 13:421–434. <https://doi.org/10.1007/s12192-008-0038-0>
- Pokatayev, V., N. Hasin, H. Chon, S.M. Cerritelli, K. Sakhuja, J.M. Ward, H.D. Morris, N. Yan, and R.J. Crouch. 2016. RNase H2 catalytic core Aicardi-Goutières syndrome-related mutant invokes cGAS-STING innate immune-sensing pathway in mice. *J. Exp. Med.* 213:329–336. <https://doi.org/10.1084/jem.20151464>
- Prakriya, M., and R.S. Lewis. 2015. Store-operated calcium channels. *Physiol. Rev.* 95:1383–1436. <https://doi.org/10.1152/physrev.00020.2014>
- Srikanth, S., J.S. Woo, B. Wu, Y.M. El-Sherbiny, J. Leung, K. Chupradit, L. Rice, G.J. Seo, G. Calmettes, C. Ramakrishna, et al. 2019. The Ca²⁺ sensor STIM1 regulates the type I interferon response by retaining the signaling adaptor STING at the endoplasmic reticulum. *Nat. Immunol.* 20: 152–162. <https://doi.org/10.1038/s41590-018-0287-8>
- Sun, L., J. Wu, F. Du, X. Chen, and Z.J. Chen. 2013. Cyclic GMP-AMP synthase is a cytosolic DNA sensor that activates the type I interferon pathway. *Science.* 339:786–791. <https://doi.org/10.1126/science.1232458>
- Warner, J.D., R.A. Irizarry-Caro, B.G. Bennion, T.L. Ai, A.M. Smith, C.A. Miner, T. Sakai, V.K. Gonugunta, J. Wu, D.J. Platt, et al. 2017. STING-associated vasculopathy develops independently of IRF3 in mice. *J. Exp. Med.* 214:3279–3292. <https://doi.org/10.1084/jem.20171351>

- Wu, J., L. Sun, X. Chen, F. Du, H. Shi, C. Chen, and Z.J. Chen. 2013. Cyclic GMP-AMP is an endogenous second messenger in innate immune signaling by cytosolic DNA. *Science*. 339:826–830. <https://doi.org/10.1126/science.1229963>
- Wu, J.-J., W. Li, Y. Shao, D. Avey, B. Fu, J. Gillen, T. Hand, S. Ma, X. Liu, W. Miley, et al. 2015. Inhibition of cGAS DNA sensing by a herpesvirus virion protein. *Cell Host Microbe*. 18:333–344. <https://doi.org/10.1016/j.chom.2015.07.015>
- Yan, N. 2017. Immune diseases associated with TREX1 and STING dysfunction. *J. Interferon Cytokine Res.* 37:198–206. <https://doi.org/10.1089/jir.2016.0086>
- Yan, N., A.D. Regalado-Magdos, B. Stiggelbout, M.A. Lee-Kirsch, and J. Lieberman. 2010. The cytosolic exonuclease TREX1 inhibits the innate immune response to human immunodeficiency virus type 1. *Nat. Immunol.* 11:1005–1013. <https://doi.org/10.1038/ni.1941>
- Yang, H., H. Wang, J. Ren, Q. Chen, and Z.J. Chen. 2017. cGAS is essential for cellular senescence. *Proc. Natl. Acad. Sci. USA*. 114:E4612–E4620. <https://doi.org/10.1073/pnas.1705499114>
- Zhang, J., H. Feng, J. Zhao, E.R. Feldman, S.-Y. Chen, W. Yuan, C. Huang, O. Akbari, S.A. Tibbetts, and P. Feng. 2016. I κ B kinase ϵ is an NFATc1 kinase that inhibits T cell immune response. *Cell Reports*. 16:405–418. <https://doi.org/10.1016/j.celrep.2016.05.083>
- Zhang, X., H. Shi, J. Wu, X. Zhang, L. Sun, C. Chen, and Z.J. Chen. 2013. Cyclic GMP-AMP containing mixed phosphodiester linkages is an endogenous high-affinity ligand for STING. *Mol. Cell*. 51:226–235. <https://doi.org/10.1016/j.molcel.2013.05.022>